AIAA JOURNAL
Vol. 30, No. 5, May 1992

Characteristic-Based Algorithms for Flows in Thermochemical Nonequilibrium

Robert W. Walters,* Pasquale Cinnella,† and David C. Slack‡
Virginia Polytechnic Institute and State University, Blacksburg, Virginia 24061
and
David Halt§
McDonnell Douglas Corporation, St. Louis, Missouri 63166

Novel numerical techniques based upon Steger-Warming, Van Leer, and Roe-type flux splittings are presented in three-dimensional generalized coordinates for the Navier-Stokes equations governing flows out of chemical and thermal equilibrium. Attention is placed on convergence to steady-state solutions with fully coupled chemistry. Time integration schemes including explicit m-stage Runge-Kutta, implicit approximate-factorization, relaxation, and LU decomposition are investigated and compared in terms of residual reduction per unit of CPU time. Practical issues such as code vectorization and memory usage on modern supercomputers are discussed.

Introduction

THE development of algorithms for the Euler and Navier-Stokes equations with thermochemical nonequilibrium effects has been spurred to a large extent by the desire to build the National Aerospace Plane (NASP) and other hypersonic vehicles. The gas dynamic models required to span the flight envelope for such a vehicle range from perfect gas to chemical nonequilibrium and, in some instances, thermal nonequilibrium models. Candler,[1,2] Liu and Vinokur,[3] Grossman and Cinnella,[4] and Wada et al.[5] are among those authors who have dealt with both thermal and chemical nonequilibrium flows, and several investigators have developed computer codes with the capability for simulating portions of this wide range of flight conditions.[6-11]

The purpose of this paper is to present a unified formulation for solving the three-dimensional Navier-Stokes equations in generalized coordinates, when arbitrary mixtures of thermally perfect gases are considered and allowed to be in *any* local thermochemical state, namely full nonequilibrium, chemical nonequilibrium, chemical equilibrium, or frozen. Consequently, the whole flight envelope of a typical hypersonic vehicle can be efficiently studied using only one code. To this end, flux-split techniques of the Steger-Warming, Van Leer, and Roe types are derived and applied to the simulation of physically challenging flow problems. The three-dimensional, finite volume computer code that has been developed under this effort has been named GASP (General Aerodynamic Simulation Program). It is highly modular and, like SPARK,[9] incorporates a generalized chemistry package. The thermal and chemical nonequilibrium model is the one proposed by Grossman and Cinnella.[4] Similar to the codes described by Palaniswamy, Chakravarthy, and Ota,[6] and Hoffman,[7] memory allocation is performed dynamically. Through the input deck, the user can select the accuracy of the spatial approximation, the flux split scheme, the type of limiter, the time integration scheme (currently, this includes m-stage Runge-Kutta, hybrid AF/relaxation, and LU/relaxation with various options; e.g., frozen Jacobians), the boundary conditions, the dimensionality of the problem (two-dimensional, axisymmetric, or three-dimensional) along with other input options. The code is highly vectorized, particularly in $j-k$ planes in an ijk logical coordinate system. A more thorough description of GASP can be found in Walters, Cinnella, and Slack[12] and in the GASP User's Guide.[13]

In the following, a brief description of the chemistry and thermodynamics models employed in this study precedes the introduction of the Navier-Stokes equations, written in vector form. The thermochemical nonequilibrium flux-split schemes in three-dimensional generalized coordinates are presented, and followed by a discussion of the time integration schemes. Results for an axisymmetric diffuser with both air and hydrogen-air chemistry, a blunt body flow, and a hydrogen-air combustion problem are detailed to provide the reader with a flavor of the capabilities of the present algorithms.

Gas Models

Chemistry Models

At high temperatures, chemical reactions will occur in gas flows resulting in changes in the amount of mass of each chemical species. In a general mixture of N species there will be J reactions taking place

$$\nu'_{1,j}X_1 + \nu'_{2,j}X_2 + \cdots + \nu'_{N,j}X_N \rightleftharpoons \nu''_{1,j}X_1 + \nu''_{2,j}X_2 + \cdots + \nu''_{N,j}X_N, \quad j = 1, 2, \ldots, J \tag{1}$$

where the $\nu'_{i,j}$ and the $\nu''_{i,j}$ are the stoichiometric coefficients of the reactants and products of species i in the jth reaction, respectively. For nonequilibrium chemistry, the rate of production of species i may be written as:

$$\dot{w}_i \equiv \frac{\mathrm{d}\rho_i}{\mathrm{d}t} = \mathcal{M}_i \sum_{j=1}^{J} (\nu''_{i,j} - \nu'_{i,j}) \left[k_{f,j} \prod_{l=1}^{N} \left(\frac{\rho_l}{\mathcal{M}_l}\right)^{\nu'_{l,j}} - k_{b,j} \prod_{l=1}^{N} \left(\frac{\rho_l}{\mathcal{M}_l}\right)^{\nu''_{l,j}} \right] \quad i = 1, 2, \ldots, N \tag{2}$$

Presented as Paper 90-0393 at the AIAA 28th Aerospace Sciences Meeting, Reno, NV, Jan. 8-11, 1990; received Nov. 28, 1990; revision received Aug. 16, 1991; accepted for publication Aug. 19, 1991.

*Associate Professor, Aerospace and Ocean Engineering, 215 Randolph Hall. Senior Member AIAA.
†Research Assistant; currently, Assistant Professor, Mississippi State Univ., Aerospace Engineering, P.O. Drawer 6176, Mississippi State Univ., MS 39762. Member AIAA.
‡Research Assistant; currently, Research Scientist, AeroSoft, Inc., P.O. Box 11334, Blackburg, VA 24062.
§Research Assistant, Mail Code 0341260, P.O. Box 516. Senior Member AIAA.

where ρ_l is the mass density and $\mathcal{M}_l$ is the mass per mole (molecular weight) of species l, and for the jth reaction the forward and backward reactions rates $k_{f,j}$ and $k_{b,j}$, are assumed to be known functions of temperature.

The frozen chemistry model is obtained from the previous one in the limit of zero rates of reaction, which amounts to zero species rates of production. The equilibrium model is obtained in the limit of infinite rates of reaction, which is accomplished in practice by multiplying the nonequilibrium values by a factor of 10^6. There are more efficient ways of performing calculations using a local chemical equilibrium assumption,[14] and some of them are being considered for implementation in GASP.

Thermodynamic Models

Following the work of Grossman and Cinnella,[4] at high temperatures the internal energy per unit mass of each species is assumed to be the sum of two portions, one in thermodynamic equilibrium and one in a nonequilibrium state, the latter being modeled by appropriate production rates. Consequently, for a generic species i

$$e_i = \tilde{e}_i(T) + e_{ni} \tag{3}$$

where $\tilde{e}_i$ is the known equilibrium portion of the energy, T is the translational temperature, and e_{ni} is the portion of the internal energy that is not in thermodynamic equilibrium. A more general formulation would include a portion of the energy as a function of the electron temperature.[3]

It is convenient to express $\tilde{e}_i$ in terms of the specific heat at constant volume, $\tilde{c}_{v_i} = \mathrm{d}\tilde{e}_i/\mathrm{d}T$, as follows:

$$\tilde{e}_i = \int_{T_{\mathrm{ref}}}^{T} \tilde{c}_{v_i}(\tau)\,\mathrm{d}\tau + h_{f_i} \tag{4}$$

where h_{f_i} is the heat of formation of species i.

If the first M out of N species in a gas mixture are assumed to contain a nonequilibrium energy contribution, the internal energy per unit mass of the mixture becomes:

$$e = \sum_{i=1}^{N} \frac{\rho_i}{\rho} e_i = \sum_{i=1}^{N} \frac{\rho_i}{\rho} \tilde{e}_i + \sum_{i=1}^{M} \frac{\rho_i}{\rho} e_{ni} \tag{5}$$

Then, the mixture reduced specific heats and gas constant can be defined by means of the usual mixture rule, as follows:

$$\tilde{c}_v \equiv \sum_{i=1}^{N} \frac{\rho_i}{\rho} \tilde{c}_{v_i}, \quad \tilde{c}_p \equiv \sum_{i=1}^{N} \frac{\rho_i}{\rho} \tilde{c}_{p_i}$$

$$\tilde{R} \equiv \sum_{i=1}^{N} \frac{\rho_i}{\rho} R_i = \tilde{c}_p - \tilde{c}_v \tag{6a,b,c}$$

and it is possible to define

$$\tilde{\gamma} \equiv \frac{\tilde{c}_p}{\tilde{c}_v} \tag{7}$$

A thermodynamic equilibrium model is easily obtained from the previous relations when the nonequilibrium contributions are set to zero. The usual perfect gas model is just a particular example of an equilibrium model, obtained when all of the species specific heats are constant (in addition to the assumption of no chemical activity).

The models that are utilized in the simulations presented in this study include the Simplified Vibrational Nonequilibrium (SVNE) and the Simplified Vibrational Equilibrium (SVE) models, which employ harmonic oscillators to account for the vibrational contribution to the species internal energy.[4] Moreover, another equilibrium model based upon a polynomial curve fit $\tilde{c}_{v_i}$ will be utilized,[15] and denoted by CF.

Equations of State

For conditions in which each individual species behaves as a thermally perfect gas, the *thermal* equation of state will relate pressure to translational temperature, in agreement with Dalton's law:

$$p = \sum_{i=1}^{N} \rho_i R_i T = \rho \tilde{R} T \tag{8}$$

where the density of the mixture is:

$$\rho = \sum_{i=1}^{N} \rho_i \tag{9}$$

The state relationship of the pressure to the specific internal energy occurs implicitly through the temperature. For a given chemical composition, internal energy, and nonequilibrium energy, the temperature must be evaluated from the *caloric* equation of state:

$$e = \sum_{i=1}^{N} \frac{\rho_i}{\rho} \left[\int_{T_{\mathrm{ref}}}^{T} \tilde{c}_{v_i}(\tau)\,\mathrm{d}\tau + h_{f_i} \right] + \sum_{i=1}^{M} \frac{\rho_i}{\rho} e_{ni} \tag{10}$$

Iterative procedures are then used to solve for T. Once T is found, the pressure is determined from Eq. (8).

Frozen Speed of Sound

The frozen speed of sound has been shown to play a key role in the establishment of the basic gasdynamic properties of flows in thermochemical nonequilibrium.[4] It is defined as:

$$a^2 \equiv \left(\frac{\partial p}{\partial \rho} \right)_{s,\rho_i/\rho,e_{ni}} \tag{11}$$

where s is the entropy per unit mass. Clarke and McChesney[16] showed that:

$$a^2 = \tilde{\gamma} \tilde{R} T = \tilde{\gamma} \left(\frac{p}{\rho} \right) \tag{12}$$

where the featured $\tilde{\gamma}$ is the ratio of specific heats corresponding to the equilibrium portion of the internal energy, defined in Eq. (7).

Governing Equations

The governing equations for a three-dimensional flow with nonequilibrium chemistry and nonequilibrium internal energy can be written in vector conservation form and generalized coordinates, as follows:

$$\frac{\partial}{\partial t} \left(\frac{\boldsymbol{Q}}{J} \right) + \frac{\partial (\hat{\boldsymbol{F}} - \hat{\boldsymbol{F}}_v)}{\partial \xi} + \frac{\partial (\hat{\boldsymbol{G}} - \hat{\boldsymbol{G}}_v)}{\partial \eta} + \frac{\partial (\hat{\boldsymbol{H}} - \hat{\boldsymbol{H}}_v)}{\partial \zeta} = \frac{\boldsymbol{W}}{J} \tag{13}$$

where $\boldsymbol{Q}$ is the vector of conserved variables and $\boldsymbol{W}$ is the vector of production rates

$$\boldsymbol{Q} = \begin{bmatrix} \rho_1 \\ \rho_2 \\ \vdots \\ \vdots \\ \vdots \\ \rho_N \\ \rho u \\ \rho v \\ \rho w \\ \rho_1 e_{n1} \\ \vdots \\ \vdots \\ \rho_M e_{nM} \\ \rho e_0 \end{bmatrix} \tag{14a}$$

$$\boldsymbol{W} = \begin{bmatrix} \dot{w}_1 \\ \dot{w}_2 \\ \vdots \\ \dot{w}_N \\ 0 \\ 0 \\ 0 \\ \rho_1 \dot{e}_{n1} + e_{n1}\dot{w}_1 \\ \vdots \\ \rho_M \dot{e}_{nM} + e_{nM}\dot{w}_M \\ 0 \end{bmatrix} \tag{14b}$$

and the inviscid flux vectors are $\hat{\boldsymbol{F}}$, $\hat{\boldsymbol{G}}$, $\hat{\boldsymbol{H}}$, with $\hat{\boldsymbol{F}}$ given as:

$$\hat{\boldsymbol{F}} = \frac{|\nabla\xi|}{J} \begin{bmatrix} \rho_1 \tilde{u} \\ \rho_2 \tilde{u} \\ \vdots \\ \rho_N \tilde{u} \\ \rho u \tilde{u} + \tilde{\xi}_x p \\ \rho v \tilde{u} + \tilde{\xi}_y p \\ \rho w \tilde{u} + \tilde{\xi}_z p \\ \rho_1 e_{n1} \tilde{u} \\ \vdots \\ \rho_M e_{nM} \tilde{u} \\ \rho \tilde{u} h_0 \end{bmatrix} \tag{15}$$

and $\hat{\boldsymbol{G}}$, $\hat{\boldsymbol{H}}$ given by similar expressions, once the appropriate contravariant velocity components and generalized coordinates are chosen. In the above, u, v, w are the Cartesian velocity components, h_0 is the stagnation enthalpy per unit mass, e_{ni} is the species nonequilibrium portion of the internal energy, and $\dot{e}_{ni}$ is its relaxation rate, which depends upon the specific nonequilibrium model.[4] Also, J is the Jacobian of the transformation

$$J = \frac{\partial(\xi,\eta,\zeta)}{\partial(x,y,z)} \tag{16}$$

and $\tilde{u}$, $\tilde{v}$, $\tilde{w}$ are the contravariant velocity components

$$\begin{pmatrix} \tilde{u} \\ \tilde{v} \\ \tilde{w} \end{pmatrix} = \begin{pmatrix} \tilde{\xi}_x & \tilde{\xi}_y & \tilde{\xi}_z \\ \tilde{\eta}_x & \tilde{\eta}_y & \tilde{\eta}_z \\ \tilde{\zeta}_x & \tilde{\zeta}_y & \tilde{\zeta}_z \end{pmatrix} \begin{pmatrix} u \\ v \\ w \end{pmatrix} \tag{17}$$

where the *normalized* gradients in the ξ, η, ζ directions have been utilized. The viscous flux vectors $\hat{\boldsymbol{F}}_v$, $\hat{\boldsymbol{G}}_v$, $\hat{\boldsymbol{H}}_v$ for the full Navier-Stokes equations, along with more details on the modeling of the viscous terms, are given by Walters et al.[13,17]

Equation (13) represents $N + M + 4$ conservation equations, with the first N corresponding to species continuity, followed by momentum conservation, M nonequilibrium energy conservation equations, and the total energy conservation equation. The system is completed by the density definition, Eq. (9), and the equations of state, Eqs. (8) and (10).

It is important to point out that the equations presented can be utilized for the study of many flowfields that are physically less challenging than a full thermochemical nonequilibrium situation. In particular, thermodynamic equilibrium is obtained by setting M to zero and dropping the nonequilibrium energy equations. Frozen flows for cases where diffusion is important can be modeled by dropping the vector of source terms. The "usual" Navier-Stokes equations for a perfect gas flow can be recovered by setting $N = 1$, $M = 0$ and simplifying the thermochemical model correspondingly.

Flux Splitting

In the following, some novel characteristic-based algorithms for the accurate numerical simulation of flows in thermochemical nonequilibrium are presented. They represent the extension to three space dimensions and generalized coordinates of the techniques derived by Grossman and Cinnella[4] in a one-dimensional context.

Although fully general, the schemes proposed reduce nicely to the simpler forms necessary for the computation of flows in thermodynamic equilibrium or even for frozen and perfect-gas-type flows, following the same guidelines outlined in the previous section.

Steger-Warming Flux Vector Splitting

Using the homogeneity property of the governing equations, Steger and Warming[18] developed a flux-vector splitting for perfect gases. This approach was extended to equilibrium flows by several authors,[19-21] and, more recently, to one-dimensional flows in thermochemical nonequilibrium.[4]

The essential feature of this approach is to diagonalize the Jacobian matrices. After some algebraic rearrangement, the final result is obtained:

$$\hat{\boldsymbol{F}}^{\pm} = \left(\frac{\tilde{\gamma} - 1}{\tilde{\gamma}}\right) \rho\lambda_A^{\pm}\hat{\boldsymbol{F}}_A + \frac{1}{2\tilde{\gamma}} \rho\lambda_B^{\pm}\hat{\boldsymbol{F}}_B + \frac{1}{2\tilde{\gamma}} \rho\lambda_C^{\pm}\hat{\boldsymbol{F}}_C \tag{18}$$

where:

$$\hat{\boldsymbol{F}}_A = \frac{|\nabla\xi|}{J} \begin{bmatrix} \rho_1/\rho \\ \rho_2/\rho \\ \vdots \\ \rho_N/\rho \\ u \\ v \\ w \\ \rho_1 e_{n1}/\rho \\ \vdots \\ \rho_M e_{nM}/\rho \\ h_0 - a^2/(\tilde{\gamma} - 1) \end{bmatrix} \tag{19a}$$

$$\hat{\boldsymbol{F}}_{B,C} = \frac{|\nabla\xi|}{J} \begin{bmatrix} \rho_1/\rho \\ \rho_2/\rho \\ \vdots \\ \rho_N/\rho \\ u \pm \tilde{\xi}_x a \\ v \pm \tilde{\xi}_y a \\ w \pm \tilde{\xi}_z a \\ \rho_1 e_{n1}/\rho \\ \vdots \\ \rho_M e_{nM}/\rho \\ h_0 \pm \tilde{u}a \end{bmatrix} \tag{19b}$$

and:

$$\lambda_A^{\pm} = \frac{\tilde{u} \pm |\tilde{u}|}{2} \tag{20a}$$

$$\lambda_B^{\pm} = \frac{\tilde{u} + a \pm |\tilde{u} + a|}{2} \tag{20b}$$

$$\lambda_C^{\pm} = \frac{\tilde{u} - a \pm |\tilde{u} - a|}{2} \tag{20c}$$

This represents a Steger-Warming-type flux vector splitting for a thermochemically active flow. The perfect gas form is obtained by setting $\rho_1/\rho = 1$, the remaining $\rho_i/\rho = 0$, and $e_{ni} = 0$. The remaining space dimensions proceed in a similar fashion.

Van Leer Flux Vector Splitting

An alternate flux vector splitting has been developed for perfect gases by Van Leer.[22] His formulation has continuously differentiable flux contributions and has been shown to result in smoother solutions near sonic points.[23] Van Leer-type splittings have been developed for equilibrium chemistry[19-21] and for nonequilibrium in one space dimension.[4] The final result in three-dimensional generalized coordinates is:

$$\hat{\boldsymbol{F}}^{\pm} = \frac{|\nabla\xi|}{J} f_m^{\pm} \begin{bmatrix} \rho_1/\rho \\ \rho_2/\rho \\ \vdots \\ \rho_N/\rho \\ u + \bar{\xi}_x[-\tilde{u} \pm 2a]/\tilde{\gamma} \\ v + \bar{\xi}_y[-\tilde{u} \pm 2a]/\tilde{\gamma} \\ w + \bar{\xi}_z[-\tilde{u} \pm 2a]/\tilde{\gamma} \\ \rho_1 e_{n_1}/\rho \\ \vdots \\ \rho_M e_{nM}/\rho \\ f_e^{\pm} \end{bmatrix} \tag{21}$$

where:

$$f_m^{\pm} = \pm\rho a \left(\frac{\pm\tilde{M} + 1}{2}\right)^2 \tag{22a}$$

$$\tilde{M} = \frac{\tilde{u}}{a} \tag{22b}$$

$$f_e^{\pm} = h_0 - m(-\tilde{u} \pm a)^2 \tag{22c}$$

Similar results hold for the other space dimensions. The above splittings are consistent with those developed by Liu and Vinokur.[3]

Preliminary calculations do not show any significant effect on the value of the parameter m in the energy equation. Also, as discussed for the Steger-Warming-type splitting, the method above can be shown to reduce to the perfect gas form.

Roe Flux Difference Splitting

The essential features of flux difference split algorithms involve the solution of local Riemann problems arising from the consideration of discontinuous states at cell interfaces on an initial data line. The scheme developed for perfect gases by Roe[24] falls into this category, and has produced excellent results for both inviscid and viscous flow simulations.[25] An extension of the Roe splitting for equilibrium chemistry has been made by several investigators.[19-21,26] This approach has been extended for the present nonequilibrium thermodynamic and chemistry model by Grossman and Cinnella[4] for one space dimension.

In the following, the *arithmetic* average of a quantity f will be denoted by:

$$\langle f \rangle = \frac{f_l + f_r}{2} \tag{23}$$

with the subscript l indicating the left state and the subscript r the right state, respectively. Also, the jump of a quantity f will be defined as:

$$[\![f]\!] = f_r - f_l \tag{24}$$

The solution of the approximate Riemann problem involves the determination of the cell interfaces fluxes as a summation over wave speeds:

$$\hat{\boldsymbol{F}}_{i+1/2} = \langle \hat{\boldsymbol{F}} \rangle - \tfrac{1}{2}([\![\hat{\boldsymbol{F}}]\!]_A + [\![\hat{\boldsymbol{F}}]\!]_B + [\![\hat{\boldsymbol{F}}]\!]_C) \tag{25}$$

where the absolute value of the wave speeds must be substituted in the formulas for the jumps in the fluxes:

$$[\![\hat{\boldsymbol{F}}]\!] = [\![\hat{\boldsymbol{F}}]\!]_A + [\![\hat{\boldsymbol{F}}]\!]_B + [\![\hat{\boldsymbol{F}}]\!]_C \tag{26}$$

Here, the $[\![\hat{\boldsymbol{F}}]\!]_A$ term corresponds to the repeated eigenvalue $\lambda_i = \hat{u}$ and may be written as:

$$[\![\hat{\boldsymbol{F}}]\!]_A = \frac{|\nabla\xi|}{J}\left([\![\rho]\!] - \frac{[\![p]\!]}{\hat{a}^2}\right)\hat{u} \begin{bmatrix} \hat{\rho}_1 \\ \hat{\rho}_2 \\ \vdots \\ \hat{\rho}_N \\ \hat{u} \\ \hat{v} \\ \hat{w} \\ \hat{e}_{n_1} \\ \vdots \\ \hat{e}_{nM} \\ \hat{h}_0 - \hat{a}^2/(\hat{\gamma} - 1) \end{bmatrix} + \frac{|\nabla\xi|}{J}\hat{\rho}\hat{u} \begin{bmatrix} [\![\rho_1/\rho]\!] \\ [\![\rho_2/\rho]\!] \\ \vdots \\ [\![\rho_N/\rho]\!] \\ [\![u]\!] - \bar{\xi}_x[\![\tilde{u}]\!] \\ [\![v]\!] - \bar{\xi}_y[\![\tilde{u}]\!] \\ [\![w]\!] - \bar{\xi}_z[\![\tilde{u}]\!] \\ [\![\rho_1 e_{n_1}/\rho]\!] \\ \vdots \\ [\![\rho_M e_{nM}/\rho]\!] \\ \Theta \end{bmatrix} \tag{27}$$

where:

$$\Theta = (\hat{u}[\![u]\!] + \hat{v}[\![v]\!] + \hat{w}[\![w]\!]) - \hat{u}[\![\tilde{u}]\!] + \sum_{j=1}^{M}\left[\!\left[\frac{\rho_j e_{nj}}{\rho}\right]\!\right] - \sum_{i=1}^{N}\hat{\psi}_i\left[\!\left[\frac{\rho_i}{\rho}\right]\!\right] \tag{28}$$

Similarly the $[\![\hat{\boldsymbol{F}}]\!]_B$ and $[\![\hat{\boldsymbol{F}}]\!]_C$ correspond to the eigenvalues $\hat{\tilde{u}} + \hat{a}$ and $\hat{\tilde{u}} - \hat{a}$, and are found to be:

$$[\![\hat{\boldsymbol{F}}]\!]_{B,C} = \frac{|\nabla\xi|}{J}\frac{1}{2\hat{a}^2}([\![p]\!] \pm \hat{\rho}\hat{a}[\![\hat{u}]\!])(\hat{\tilde{u}} \pm \hat{a}) \begin{bmatrix} \hat{\rho}_1 \\ \hat{\rho}_2 \\ \vdots \\ \hat{\rho}_N \\ \hat{u} \pm \bar{\xi}_x a \\ \hat{v} \pm \bar{\xi}_y a \\ \hat{w} \pm \bar{\xi}_z a \\ \hat{e}_{n_1} \\ \vdots \\ \hat{e}_{nM} \\ \hat{h}_0 \pm \hat{\tilde{u}}\hat{a} \end{bmatrix} \tag{29}$$

The appropriate averaged values of the flow variables $\hat{\rho}$, $\hat{u}$, $\hat{v}$, $\hat{w}$, $\hat{\rho}_i$, $\hat{e}_{nj}$, $\hat{h}_0$, $\hat{\psi}_i$ are found to be:

$$\hat{\rho} = \sqrt{\rho_r \rho_\ell} \tag{30}$$

$$\hat{u} = \frac{\langle u\sqrt{\rho}\rangle}{\langle\sqrt{\rho}\rangle} \tag{31a}$$

$$\hat{v} = \frac{\langle v\sqrt{\rho}\rangle}{\langle\sqrt{\rho}\rangle} \tag{31b}$$

$$\hat{w} = \frac{\langle w\sqrt{\rho}\rangle}{\langle\sqrt{\rho}\rangle} \tag{31c}$$

$$\hat{\rho}_i = \frac{\langle(\rho_i/\rho)\sqrt{\rho}\rangle}{\langle\sqrt{\rho}\rangle} \tag{32a}$$

$$\hat{e}_{nj} = \frac{\langle(\rho_j e_{nj}/\rho)\sqrt{\rho}\rangle}{\langle\sqrt{\rho}\rangle} \tag{32b}$$

$$\hat{h}_0 = \frac{\langle h_0\sqrt{\rho}\rangle}{\langle\sqrt{\rho}\rangle} \tag{33a}$$

$$\hat{\psi}_i = \frac{R_i\hat{T}}{\hat{\gamma} - 1} - \hat{e}_i + \frac{\hat{q}^2}{2} \tag{33b}$$

where:

$$\hat{T} = \frac{\langle T\sqrt{\rho}\rangle}{\langle\sqrt{\rho}\rangle} \tag{34a}$$

$$\hat{e}_i \equiv (\hat{\tilde{e}}_i) = \frac{\langle \tilde{e}_i\sqrt{\rho}\rangle}{\langle\sqrt{\rho}\rangle} \tag{34b}$$

$$\hat{q}^2 = \hat{u}^2 + \hat{v}^2 + \hat{w}^2 \tag{34c}$$

We also have:

$$\hat{\gamma} - 1 = \frac{\hat{R}}{\hat{c}_v^*} \tag{35}$$

where:

$$\hat{R} = \sum_{i=1}^{N} \hat{\rho}_i R_i = \frac{\langle \tilde{R}\sqrt{\rho}\rangle}{\langle\sqrt{\rho}\rangle} \tag{36a}$$

$$\hat{c}_v^* = \sum_{i=1}^{N} \hat{\rho}_i c_{vi}^* \tag{36b}$$

and

$$c_{vi}^* \equiv \frac{1}{[\![T]\!]} \int_{T_\ell}^{T_r} \tilde{c}_{vi}\, dT \tag{37}$$

The averaged contravariant velocity components are given by:

$$\begin{pmatrix} \hat{\tilde{u}} \\ \hat{\tilde{v}} \\ \hat{\tilde{w}} \end{pmatrix} = \begin{pmatrix} \tilde{\xi}_x & \tilde{\xi}_y & \tilde{\xi}_z \\ \tilde{\eta}_x & \tilde{\eta}_y & \tilde{\eta}_z \\ \tilde{\zeta}_x & \tilde{\zeta}_y & \tilde{\zeta}_z \end{pmatrix} \begin{pmatrix} \hat{u} \\ \hat{v} \\ \hat{w} \end{pmatrix} \tag{38}$$

Also, we may determine $\hat{a}$ as:

$$\hat{a}^2 = (\hat{\gamma} - 1)\left[\hat{h}_0 - \frac{\hat{q}^2}{2} + \hat{c}_v^*\hat{T} - \sum_{i=1}^{N} \hat{\rho}_i\hat{e}_i - \sum_{j=1}^{M} \hat{e}_{nj}\right] \tag{39}$$

The other space dimensions can be treated in a similar fashion.

Numerical Formulation

The governing equations presented in a previous section are discretized in space using a finite-volume approach. The inviscid fluxes at the volume boundaries are evaluated using upwind differences in conjunction with the algorithms just introduced. The viscous fluxes are determined from a standard central difference approach. More details are given by Walters et al.[13]

Time Integration

In order to obtain a steady-state solution, the spatially discretized Navier Stokes equations must be integrated in time. Three time integration methods are compared: an m-stage explicit Runge-Kutta method, an implicit LU decomposition in a plane, and an implicit Approximate Factorization (AF) in a plane.

The Runge-Kutta scheme advances the solution in time using:

$$\begin{aligned} Q^{(0)} &= Q^{(n)} \\ Q^{(1)} &= Q^{(0)} - \alpha_1 \frac{\Delta t}{V} R(Q^{(0)}) \\ Q^{(2)} &= Q^{(0)} - \alpha_2 \frac{\Delta t}{V} R(Q^{(1)}) \\ &\vdots \qquad\qquad \vdots \\ Q^{(m)} &= Q^{(0)} - \alpha_m \frac{\Delta t}{V} R(Q^{(m-1)}) \\ Q^{(n+1)} &= Q^{(m)} \end{aligned} \tag{40}$$

where:

$$R(Q) = \frac{\partial(\hat{F} - \hat{F}_v)}{\partial\xi} + \frac{\partial(\hat{G} - \hat{G}_v)}{\partial\eta} + \frac{\partial(\hat{H} - \hat{H}_v)}{\partial\zeta} - W \tag{41}$$

with the standard weighting coefficients:

$$\alpha_i = \frac{1}{m - i + 1} \tag{42}$$

and V is the cell volume ($V = 1/J$). Convergence to the steady-state is also accelerated by using the maximum permissible time-step for each individual cell in the flowfield, as dictated by local stability analysis.

The two implicit methods considered are based upon the Euler implicit time integration scheme. Both of these schemes use relaxation in the remaining direction, and have the ability to reuse the factored Jacobian matrix.[13,27]

Storage and Vectorization for LU and AF

The LU decomposition and the AF methods utilize a highly vectorized banded solver in order to save storage and CPU time. The solver stores a matrix $A(j,k)$ with ndiag super/sub

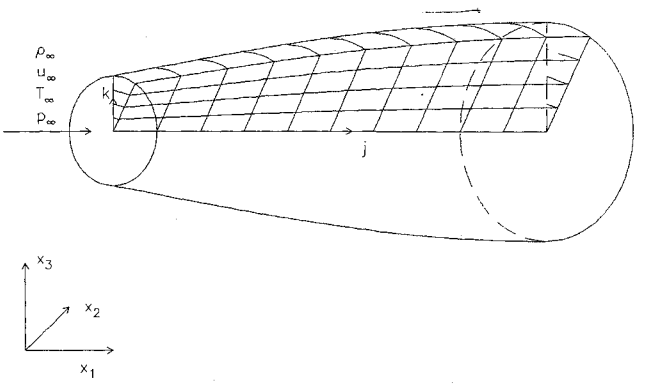

Fig. 1 Geometry of the axisymmetric nozzle and qualitative representation of the mesh.

diagonals in an array D by the rule $A(j,k)$ is stored in $D(\text{ndiag} + 1 + j - k,k)$: that is, the jth column of A goes to jth column of D and the main diagonal of A is then the ndiag + 1 row of D with each super and subdiagonal on the rows above and below that one in D.

For LU in a plane of dimension jdim × kdim with $(N + M + 4)$ conserved variables, this results in a matrix that requires storage of $(2 * \text{ndiag} + 1) * (\text{jdim} * \text{kdim}) * (N + M + 4)$ where $\text{ndiag} = (\text{jdim} + 1) * (N + M + 4) - 1$ for the jdim bandwidth case, or $\text{ndiag} = (\text{kdim} + 1) * (N + M + 4) - 1$ for the kdim bandwidth case.

For AF in a plane, the first step of the solution is done with a jdim bandwidth, and the second is done with a kdim bandwidth. In both cases, the matrix is in block tridiagonal form and requires the amount of storage given for the LU method but with $\text{ndiag} = 2 * (N + M + 4) - 1$. Hence, for large jdim and kdim, AF in a plane requires far less storage than LU in a plane.

In terms of vectorization, the banded matrix solver vectorizes over the length of the dot product involved in the LU decomposition phase and the forward/backward substitution phases. In addition, for the AF algorithm, since the η and ζ directions are decoupled, both steps in the solution process can be divided into independent sections of length jdim and kdim, respectively. The algorithm can then be further vectorized over these sections resulting in substantial CPU savings.

Numerical Results

A few numerical examples of flow computations are included, in order to illustrate the accuracy and efficiency of the methodology presented. The test cases include the inviscid, steady flow in a supersonic nozzle, a hypersonic, laminar flow over an axisymmetric blunt body with air chemistry, and a turbulent, hydrogen-air combustion problem.

The numerical results presented here have been obtained using the flux-vector and flux-difference splitting techniques previously summarized. For the supersonic cases, all splittings yield the same predictions within plotting accuracy. However, this is not always the case, especially when in the presence of contact discontinuities and shear layers, where Roe's technique yields more accurate results for perfect gas calculations.[25]

Nozzle with Air Chemistry

The axisymmetric nozzle shown in Fig. 1 has a geometry defined by the radius $r = 0.125L[1 + \sin(\pi x/2L)]$, with a length $L = 2$ m and $0 \le x \le L$.

Using the chemical model for high-temperature air described by Park,[28] numerical solutions have been obtained for the following inlet conditions: $p = 1.95256\ 10^5$ N/m^2, $T = 9000$ K, $u = 4000$ m/s, $v = w = 0$, and an equilibrium mass fraction distribution. Results are presented for an axisymmetric 2 × 6 × 41 grid, using Steger-Warming, Van Leer, and Roe algorithms. The predictions from the different algorithms coincide within plotting accuracy for this fully supersonic case. At each axial location, the values have been area-averaged in the transverse direction. The resulting curves compare very well with the one-dimensional results of Grossman and Cinnella.[4] For this problem, there are non-negligible gradients of chemical and flow properties in the transverse direction.

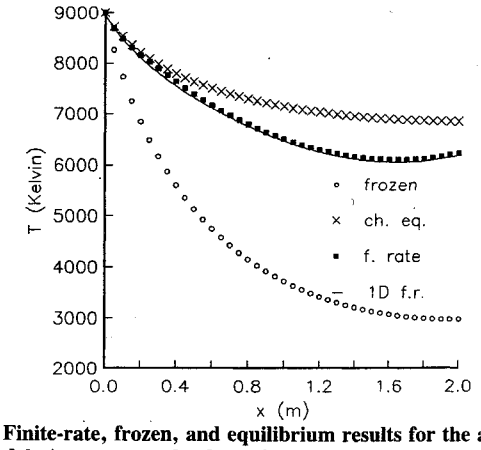

Fig. 2 Finite-rate, frozen, and equilibrium results for the air chemistry model. Area-averaged values of temperature are compared with one-dimensional results.

The effect of assuming a frozen chemistry or a local chemical equilibrium for the same problem is investigated in Fig. 2, where the SVE thermodynamic model was used. The temperature predictions vary significantly, with the finite-rate calculations lying in the middle of the two limiting cases. Some of the *mechanical* quantities, such as pressure and velocity, are hardly affected by the differences in the chemical behaviour. The mass fractions, however, which are constant for frozen calculations, are significantly changed by the assumption of local chemical equilibrium. As already discussed in a previous section, the equilibrium predictions were obtained by multiplying the rate constants by a factor of 10^6 and running the finite-rate code. It may be useful to point out that a calculation with a factor of 10^{12} did not change the results.

A plot of the normalized residual vs CPU time for the air chemistry case and different time integration algorithms is presented in Fig. 3. All computations have been performed

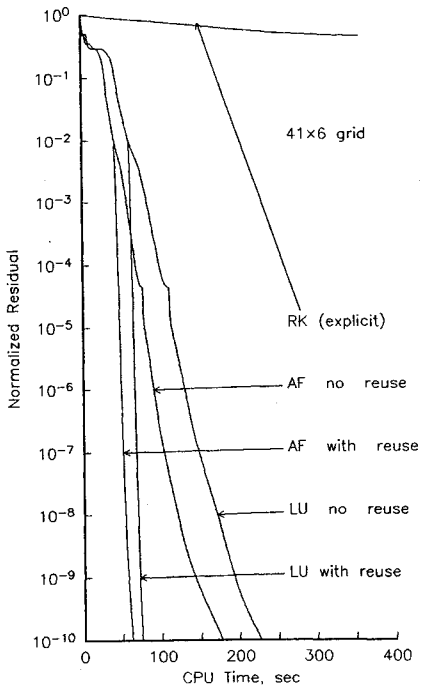

Fig. 3 Convergence history for the air chemistry model on a Cray-YMP machine.

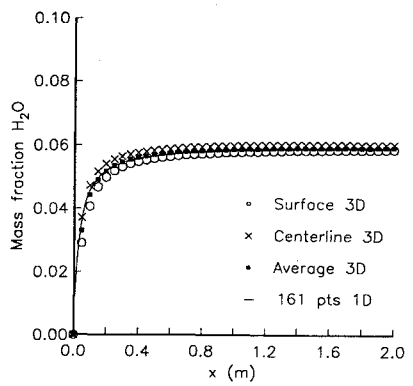

Fig. 4 Results for the hydrogen-air chemistry model. Surface, centerline, and area-averaged values of H_2O are compared.

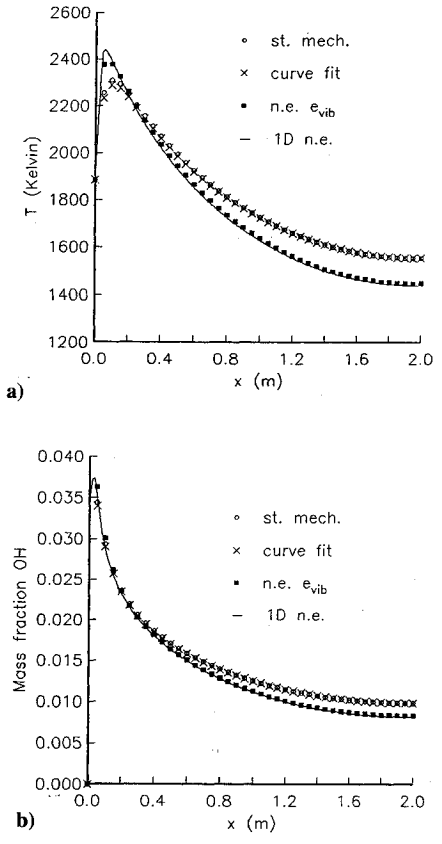

Fig. 5 Comparison of several thermodynamic models for the hydrogen-air chemistry model. *st. mech* = Equilibrium vibrational energy (SVE); *curve fit* = Curve fit c_{vi} (CF); *n.e.* e_{vib} = Nonequilibrium vibrational energy (SVNE); *1D n.e.* = Quasi-one-dimensional result with SVNE. a) Temperature; b) Mass fraction OH.

on a Cray-YMP machine, with a residual reduction of 10^{-10} as a convergence criterion. The explicit second-order Runge-Kutta algorithm turned out to be completely inadequate, due to the severe restrictions on its stability brought about by the chemical *stiffness*. The curve shown has been obtained with a CFL number of 0.1. A CFL number of 100 has been used for both the LU decomposition and AF methods. A further reduction of CPU time has been obtained by means of a reuse of the decomposition elements for both implicit schemes, beginning after a residual reduction of two orders of magnitude.

Nozzle with Hydrogen-Air Chemistry

Using the Rogers and Chinitz hydrogen-air chemistry model,[29] numerical solutions have been obtained for the same nozzle and the following inlet conditions: $p = 0.8026\ 10^5$ N/m^2, $T = 1884.3$ K, $u = 1245$ m/s, $v = w = 0$. The initial composition of the flow consists of an equivalence ratio Φ, the ratio of the mass fraction of H_2 to the mass fraction of O_2, normalized by the stoichiometric ratio, of $\Phi = 0.29841$. This composition causes very steep concentration gradients near the inlet of the duct. The results are presented in Fig. 4 for the same axisymmetric grid. Once again, the averaged values compare very well with the one-dimensional results.

A comparison between different thermodynamic models is shown in Fig. 5. Results obtained using the SVE model are plotted along with the predictions of the CF and SVNE models. In addition, the SVNE results obtained with a quasi-one-dimensional code are shown. It can be noticed that there is a noticeable freezing of vibrational energy in the nonequilibrium predictions. Both equilibrium models are in excellent agreement, due to the moderate temperatures. The discrepancy in the temperature prediction affects the intermediate step of the combustion, the production of OH, but does not alter the final level of water mass fraction.

A plot of the normalized residual versus number of iterations and CPU time for the hydrogen-air chemistry case and different time integration algorithms is presented in Fig. 6. Here, the Runge-Kutta algorithm was limited to a CFL num-

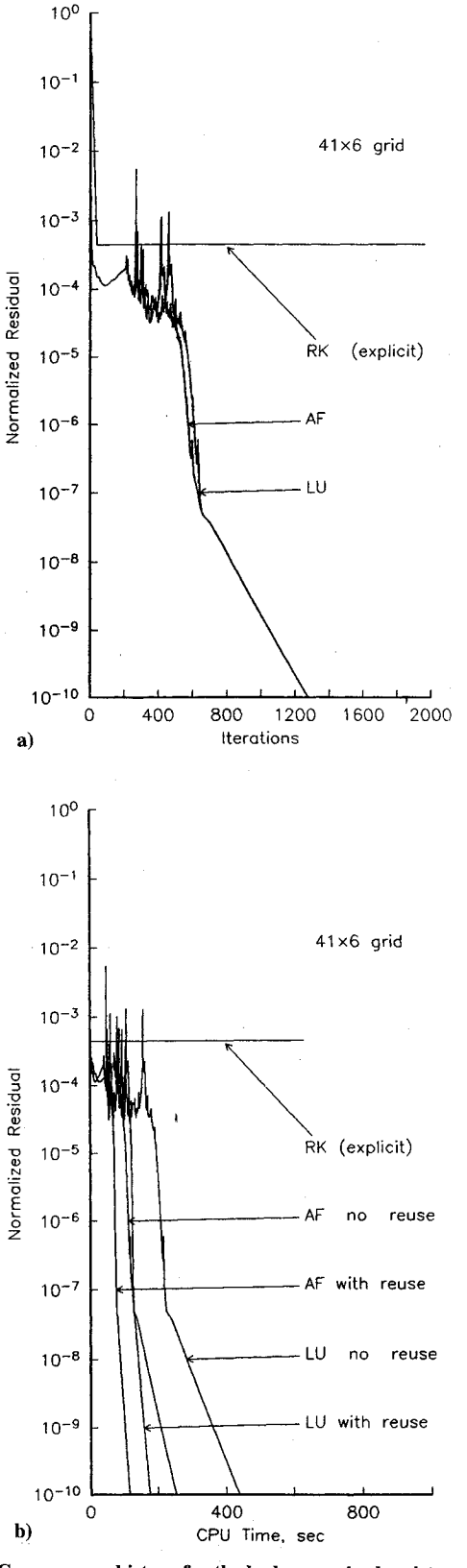

Fig. 6 Convergence history for the hydrogen-air chemistry model on a Cray-YMP machine. a) Residual reduction vs iteration number. b) Residual reduction vs CPU time.

ber of 10^{-4}, due to the *extreme* stiffness of the two-reaction model. The LU and AF algorithms, as well as the reuse strategies discussed, used a CFL of 100. Examination of the plot of residual vs iteration number in Fig. 6 shows little difference between the AF and LU algorithms. This is likely due to the predominance of the diagonal terms in the algebraic problem, associated with the chemical source terms Jacobians for these test cases.

RAM-C II Test Case

In the late sixties, the Radio Attenuation Measurement (RAM) tests were conducted in order to obtain data in a velocity regime in which ionization could not be neglected. Probes were instrumented in order to obtain electron number densities. Details of these tests can be found in Jones and Cross.[30] The second in the series of flights, referred to as the RAM-C II test, has become a popular test case for modern computational fluid dynamics algorithms[31–33] because no ablation products were produced.

The geometry consists of a sphere-cone with a 15.24 cm nose radius and a 9 deg cone half-angle. A grid containing 31 points along the body and 41 points radially was generated. This grid was then rotated through an angle of $\pi/40$ in order to yield an appropriate grid for an axisymmetric calculation. The case considered here corresponds to a flight altitude of 61 km with freestream conditions: T_∞ = 254 K, U_∞ = 7650 m/s, and a Reynolds number based on the nose radius Re_n = 19,500. These conditions correspond to a flight Mach number M_∞ = 23.9. A laminar calculation was performed with a cell Reynolds number based on the minimum mesh spacing $Re_c \approx 4$. The wall temperature was held fixed at 1500 K. Park air chemistry with 7 species (N_2, O_2, NO, NO^+, N, O, e^-) and 18 reactions was used as the chemistry model.[28]

Fig. 7 shows computed Mach number contours from the numerical solution using the Van Leer type of flux vector splitting developed earlier. Peak electron number densities obtained with both the Van Leer and the Roe flux formulas are compared to experiment in Fig. 8. On this mesh, both methods overpredict the data on the aft portion of the body. It is interesting to note that nonphysical behavior and convergence problems were observed if the flowfield was initialized to the freestream Mach number of 23.9. In this case, the shock wave forms on the body and then moves *outward* into the field, resulting in a severe transient that limited the time-step. However, by initializing the flow to a low Mach number (0.1, in this case) and enforcing freestream conditions at the outer boundary, the shock moves *inward* toward the body, which results in much better numerical behavior. The maximum Courant number achieved during this simulation was 66. This problem is referred to as GASP Test Case 13, and like all other GASP test cases, is available on-line at NASA Langley and Ames.

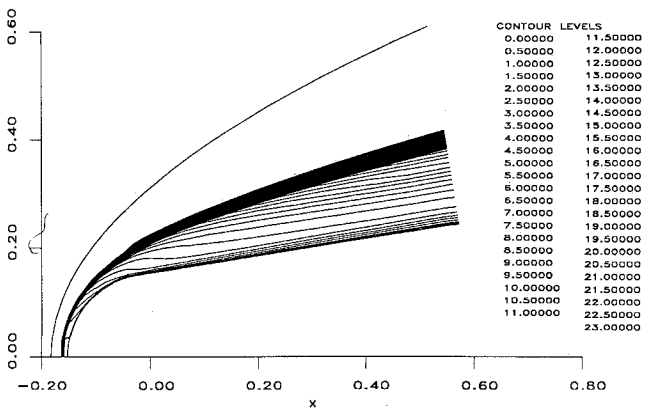

Fig. 7 Mach number contours for the RAM-C II at 61 km.

Hydrogen-Air Example

As a final demonstration of the characteristic-based, thermochemical nonequilibrium algorithms developed in this paper, a problem involving the chemical kinetics of a hydrogen-air combustion process is considered in which turbulent mixing plans an important role. A sketch of the problem is shown in Fig. 9 in which a Mach 2.44 vitiated air stream at 1270 K mixes with a sonic jet of H_2 at 254 K. The mass fractions of the vitiated air stream at the entrance were taken to be 0.486, 0.258, and 0.256 for N_2, O_2, and H_2O respectively. The wall temperature was held fixed at 298 K and the Baldwin and Lomax algebraic turbulence model was employed. Details of the experimental investigation of this problem are reported by Burrows and Kurkov.[34]

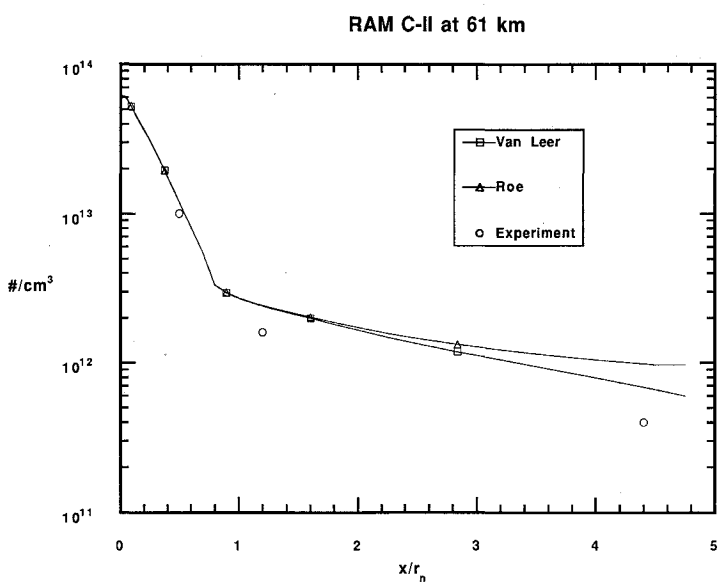

Fig. 8 Comparison of computed and experimental peak electron number density.

In all of the computations, 81 points were used in the normal direction. In the streamwise direction, both 21 and 41 points were used in order to assess the effect of any streamwise gradients on the numerical solution. Two different chemical models were used; the Evans and Schexnayder (labeled E&S) model,[35] which contains 12 species and 25 reactions and the Drummond model[36] with nine species and 18 reactions. Figs. 10 and 11 show the water mole fraction and total temperature profiles in the exit plane compared to the experiment. The computed results are very similar to the results of Kamath[37] in that the location of the peaks from the numerical solutions are closer to the lower wall than the experimental data. This is probably due to the fact that uniform profiles of all quantities were specified at the inflow in lieu of accounting for turbulent boundary layer profiles at that station.

The only noticable effect of the streamwise grid refinement is a sharpening of the profile peaks in the exit plane, although the location of the peaks is unchanged. These calculations were performed with GASP in PNS mode with the implicit LU scheme. On the 21 × 81 × 2 mesh, it is noted that the Evans and Schexnayder model runs to completion in 224 seconds at a CFL equal to 10 on the NAS Cray-YMP, whereas the Drummond model required 374 seconds due to the fact that the maximum CFL was 4 (without user intervention). These two calculations are referred to as GASP Test Case 12a (E&S) and Test Case 12b (Drummond) in the on-line documentation.

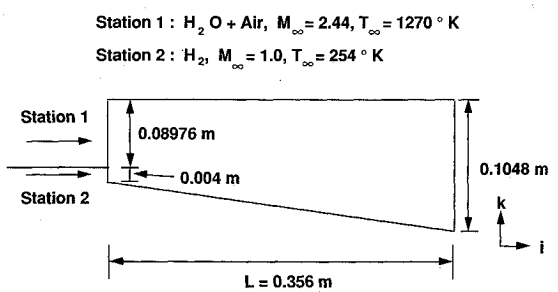

Fig. 9 Sketch of the Burrows and Kurkov hydrogen-air combustion problem.

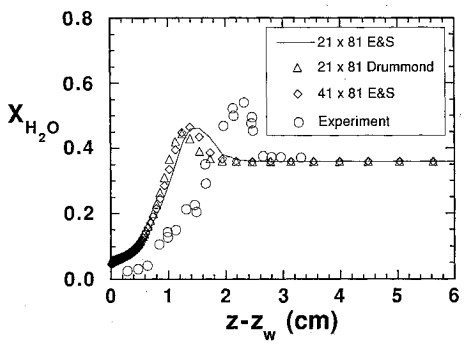

Fig. 10 Computed and experimental H_2O mole fraction profiles at $x = 0.356$ m.

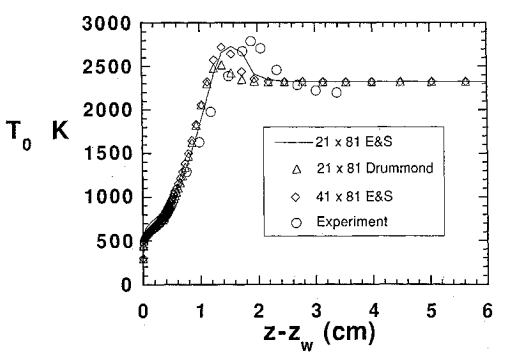

Fig. 11 Computed and experimental total temperature profiles at $x = 0.356$ m.

Concluding Remarks

The development of flux-split techniques for the numerical simulation of multidimensional flowfields in thermochemical nonequilibrium has been described. The approach undertaken is fully general and may be used to investigate virtually any problem involving mixtures of thermally perfect gases at high temperature and/or high velocity.

Acknowledgments

NASA Langley Research Center sponsored the work of R. W. Walters, P. Cinnella, and D. C. Slack under NASA Grant NAG1-776. The advice and assistance of B. Grossman were instrumental to this research effort.

References

[1]Candler, G., "On the Computation of Shock Shapes in Nonequilibrium Hypersonic Flows," AIAA Paper 89-0312, Reno, NV, 1989.

[2]Candler, G., "The Computation of Weakly Ionzied Hypersonic Flows in Thermo-Chemical Nonequilibrium," Ph.D. Dissertation, Stanford Univ., Stanford, CA, 1988.

[3]Liu, Y., and Vinokur, M., "Nonequilibrium Flow Computations: I. An Analysis of Numerical Formulations of Conservation Laws," NASA CR 177489, June 1988.

[4]Grossman, B., and Cinnella, P., "Flux-Split Algorithms for Flows with Nonequilibrium Chemistry and Vibrational Relaxation," *Journal of Computational Physics,* Vol. 88, No. 1, May 1990, pp. 131–168.

[5]Wada, Y., Kubota, H., Ogawa, S., and Ishiguro, T., "A Generalized Roe's Approximate Riemann Solver for Chemically Reacting Flows," AIAA Paper 89-0202, Reno, NV, 1989.

[6]Palaniswamy, S., Chakravarthy, S. R., and Ota, D. K., "Finite Rate Chemistry for USA-Series Codes: Formulation and Applications," AIAA Paper 89-0200, Reno, NV, 1989.

[7]Hoffman, J. J., "Development of an Algorithm for the Three-Dimensional Fully-Coupled Navier Stokes Equations with Finite Rate Chemistry," AIAA Paper 89-0670, Reno, NV, 1989.

[8]Drummond, J. P., Rogers, R. C., and Hussaini, M. Y., "A Detailed Numerical Model of a Supersonic Reacting Mixing Layer," AIAA Paper 86-1427, Huntsville, AL, 1986.

[9]Carpenter, M., "A Generalized Chemistry Version of SPARK," NASA CR 4196, 1988.

[10]Molvik, G. A., and Merkle, C. L., "A Set of Strongly Coupled, Upwind Algorithms for Computing Flows in Chemical Nonequilibrium," AIAA Paper 89-0199, Reno, NV, 1989.

[11]Krispin, J., and Anderson, J. D., "Accelerating the Computation of Steady State Solutions for Nonequilibrium, Chemically Reacting Flow Fields," AIAA Paper 88-0513, Reno, NV, 1988.

[12]Walters, R. W., Cinnella, P., and Slack, D. C., "A Status Report on GASP—A General Aerodynamic Simulation Program," *Seventh National Aero-Space Plane Symposium,* Paper 9, NASA Lewis, Cleveland, OH, 1989.

[13]Walters, R. W., Slack, D. C., Cinnella, P., Applebaum, M., and Frost, C., "A User's Guide to GASP," NASA Langley Research Center, Hampton, VA, Nov. 1991.

[14]Liu, Y., and Vinokur, M., "Equilibrium Gas Flow Computations. I. Accurate and Efficient Calculations of Equilibrium Gas Properties," AIAA Paper 89-1736, Buffalo, NY, 1989.

[15]McBride, G. J., Heimel, S., Ehlers, J. G., and Gordon, S., "Thermodynamic Properties to 6000 K for 210 Substances Involving the First 18 Elements," NASA SP-3001, 1963.

[16]Clarke, J. F., and McChesney, M., *The Dynamics of Real Gases,* Butterworth, London, 1964, p. 179.

[17]Walters, R. W., Cinnella, P., Slack, D. C., and Halt, D., "Characteristic-Based Algorithms for Flows in Thermo-Chemical Nonequilibrium," AIAA Paper 90-0393, Reno, NV, 1990.

[18]Steger, J. L., and Warming, R. F., "Flux Vector Splitting of the Inviscid Gasdynamics Equations with Application to Finite-Difference Methods," *Journal of Computational Physics,* Vol. 40, 1981, pp. 263–293.

[19]Grossman, B., and Walters, R. W., "Analysis of Flux-Split Al-

gorithms for Euler's Equations with Real Gases," *AIAA Journal,* Vol. 27, No. 5, 1989, pp. 524–531.

[20]Vinokur, M., and Liu, Y., "Equilibrium Gas Flow Computations II: An Analysis of Numerical Formulations of Conservation Laws," AIAA Paper 88-0127, Reno, NV, 1988.

[21]Liou, M.-S., Van Leer, B., and Shuen, J.-S., "Splitting of Inviscid Fluxes for Real Gases," NASA TM 100856, 1988.

[22]Van Leer, B., "Flux-Vector Splitting for the Euler Equations," *Lecture Notes in Physics,* Vol. 170, Springer-Verlag, Berlin, 1982, pp. 507–512.

[23]Anderson, W. K., Thomas, J. L., and Van Leer, B., "Comparison of Finite Volume Flux Vector Splittings for the Euler Equations," *AIAA Journal,* Vol. 24, No. 9, 1986, pp. 1453–1460.

[24]Roe, P. L., "Approximate Riemann Solvers, Parameter Vectors, and Difference Schemes," *Journal of Computational Physics,* Vol. 43, 1981, pp. 357–372.

[25]Van Leer, B., Thomas, J. L., Roe, P. L., and Newsome, R. W., "A Comparison of Numerical Flux Formulas for the Euler and Navier-Stokes Equations," AIAA Paper 87-1104-CP, Honolulu, HI, 1987.

[26]Glaister, P., "An Approximate Linearised Riemann Solver for the Euler Equations for Real Gases," *Journal of Computational Physics,* Vol. 74, 1988, pp. 382–408.

[27]Walters, R. W., Reu, T., McGrory, W. D., Thomas, J. L., and Richardson, P. F., "A Longitudinally-Patched Grid Approach with Applications to High Speed Flows," AIAA Paper 88-0715, Reno, NV, 1988.

[28]Park, C., "On Convergence of Computation of Chemically Reacting Flows," AIAA Paper 85-0247, Reno, NV, 1985.

[29]Rogers, R. C., and Chinitz, W., "Using a Global Hydrogen-Air Combustion Model in Turbulent Reacting Flow Calculations," *AIAA Journal,* Vol. 21, No. 4, 1983, pp. 586–592.

[30]Jones, W. L., and Cross, A. E., "Electrostatic-Probe Measurements of Plasma Parameters For Two Reentry Flight Experiments at 25,000 Feet Per Second," NASA TN D-6617, 1972.

[31]Candler, G. V., and MacCormack, R. W., "The Computation of Hypersonic Ionized Flows in Chemical and Thermal Nonequilibrium," AIAA Paper 88-0511, Reno, NV, 1988.

[32]Palmer, G., "The Development of an Explicit Thermochemical Nonequilibrium Algorithm and Its Application to Compute Three Dimensional AFE Flowfields," AIAA Paper 89-1701, Buffalo, NY, 1989.

[33]Kang, S., Dunn, M. G., and Jones, W. L., "Theoretical and Measured Electron-Density Distributions for the RAM Vehicle at High Altitudes," AIAA Paper 72-689, Boston, MA, 1972.

[34]Burrows, M. C., and Kurkov, A. P., "Analytical and Experimental Study of Supersonic Combustion of Hydrogen in a Vitiated Airstream," NASA TM X-2828, 1973.

[35]Evans, J. S., and Schexnayder, C. J., Jr., "Influence of Chemical Kinetics and Unmixedness on Burning in Supersonic Hydrogen Flames," *AIAA Journal,* Vol. 18, No. 2, 1979, pp. 188–193.

[36]Drummond, J. P., and Hussaini, M. Y., "Numerical Simulation of a Supersonic Reacting Mixing Layer," AIAA Paper 87-1325, Honolulu, HI, 1987.

[37]Kamath, H., "Parabolized Navier-Stokes Algorithm for Chemically Reacting Flows," AIAA Paper 89-0386, Reno, NV, 1989.